Dynamics of anisotropy on decaying homogeneous turbulence subjected to system rotation

Y. Morinishi, K. Nakabayashi, and S. Q. Ren
Department of Mechanical Engineering, Nagoya Institute of Technology, Gokiso-Cho, Showa-Ku, Nagoya 466-8555, Japan

The dynamics of the anisotropy of the Reynolds stress tensor and its behavior in decaying homogeneous turbulence subjected to system rotation are investigated in this study. Theoretical analysis shows that the anisotropy can be split into two parts: polarization and directional anisotropies. The former can be further separated into a linear part and a nonlinear part. The corresponding linear solution of the polarization anisotropy is derived in this paper. This solution is found to be equivalent to the linear solution of the anisotropy. While proposing a method to introduce the polarization anisotropy into an isotropic turbulence, direct numerical simulation (DNS) of the rotating turbulence with or without the initial anisotropy is carried out. The linear solution of the anisotropy agrees very well with the DNS result, showing that the evolution of the polarization anisotropy is mainly dominated by the linear effect of the system rotation. With an immediate rotation rate, the coupling effect between the system rotation and nonlinear interactions causes an energy transfer from the region near the pole to the region near the equator in wave space. This type of transfer causes an anisotropic distribution of the kinetic energy between the pole and equator, which relates closely to the directional anisotropy and the two-dimensionalization. In addition, we find that the presence of the initial polarization anisotropy does not affect the evolution of the directional anisotropy, while the presence of the initial directional anisotropy greatly influences the evolution of the polarization anisotropy. © *2001 American Institute of Physics.*
[DOI: 10.1063/1.1398040]

I. INTRODUCTION

Rotating flows find numerous industrial applications in engineering as well as in geophysics, astrophysics, and meteorology. The turbulence properties of the rotating flow in blade passages of radial pumps and gas or steam turbines determine the efficiency of these devices. Therefore, the study of the rotating turbulence is interesting from the viewpoints of both turbulence modeling and fundamental research. To date, a number of researchers have studied rotating turbulence that includes decaying homogeneous turbulence (e.g., Jacquin et al.[1] and Mansour et al.[2]), turbulent shear flow (e.g., Bardina et al.[3] and Salhi and Cambon[4]), and turbulent channel flow (e.g., Johnston et al.,[5] Kristoffersen and Anderson,[6] and Nakabayashi and Kitoh[7]) with theoretical, experimental, and numerical methods. These studies show that the main influences of system rotation on turbulence are three-fold.

First is the linear effect of the Coriolis term on turbulence. Any turbulence statistic with the Coriolis term in its governing equation reflects this linear effect explicitly. The classical Taylor–Proudman theorem[8] clearly illustrates this linear effect of the system rotation. Based on the linear theory, Leblanc and Cambon[9] analyzed instability features of the rotating shear flow.

The second influence is the so-called "scrambling effect" due to the nonlinear interaction between the velocity components of the rotating turbulence. A number of turbulence statistics such as kinetic energy, energy dissipation rate, and energy transfer function, are affected by the scrambling effect, though there are no explicit rotation terms in their governing equations. This effect explains why system rotation inhibits the decay of kinetic energy. Using a certain assumption, Cambon et al.[10] expressed this effect into an explicit form and showed that, the stronger the scrambling effect, the slower the decay of the kinetic energy.

The third influence is a coupling effect between the system rotation and the nonlinear interactions ("coupling effect" hereafter). It is found that, within a certain range of rotation rates, this effect is closely related to the Reynolds stress anisotropy and the two-dimensionalization phenomenon in rotating turbulence. However, this effect is subtle and remains unclear. In this paper, we divide the effect of the Coriolis force into three-fold just for discussion convenience. In fact, the three-fold effects are coexisting and affect one another. For example, the linear effect of the strong rotation finally results in the steady two-dimensional mode, but the two-dimensionalization is due to the nonlinear effect.

Our main objective in this paper is to investigate the dynamics of the anisotropy of the Reynolds stress tensor and its behavior in homogeneous decaying turbulence subjected to system rotation. Using the rapid distortion theory (RDT), Kassinos and Reynolds[11] provided a linear solution for the second-order spectral tensor of the one-point velocity correlation in rotating or axisymmetric systems. Mansour et al.[12] obtained a linear solution for the anisotropy tensor by adopting a model spectral tensor. Cambon and Jacquin[13] discussed the anisotropic behavior of the Reynolds stress tensor by

Phys. Fluids, Vol. 13, No. 10, October 2001

Dynamics of anisotropy on decaying   2913

splitting the anisotropy tensor into two parts: the directional and polarization anisotropies. For convenience, in this paper we extend the concepts of the directional and polarization anisotropies from wave space to physical space. Based on a theoretical analysis, we derive the linear solution of the anisotropy of the Reynolds stress tensor, which is also equivalent to the linear evolution of the polarization anisotropy. While proposing a method to introduce the polarization anisotropy into an initially isotropic turbulence, DNS of the rotating turbulence with or without the initial anisotropy is conducted. The linear and coupling effects of the system rotation on the anisotropic features of the Reynolds stresses are discussed. Finally, the relationship between the energy transfer and the anisotropy is also demonstrated based on the DNS results.

The remainder of this paper is arranged as follows. The governing equations of the rotating flow are given in the next section. In Sec. III we present a linear solution for the anisotropy of the Reynolds stresses. A numerical method introducing the polarization anisotropy into an initially isotropic turbulence is proposed in Sec. IV. The DNS results and discussion are given in Sec. V, in three subsections that focus, respectively, on (a) the linear effect of system rotation on an anisotropy tensor, (b) the coupling effect on anisotropy tensor, and (c) the direction of local energy transfer. In Sec. VI, we briefly summarize the present analysis.

II. GOVERNING EQUATIONS

The Navier–Stokes (N–S) and continuity equations for incompressible flow without mean velocity in a rotating system read as

$$\frac{\partial \mathbf{u}}{\partial t} + 2\mathbf{\Omega} \times \mathbf{u} = -\nabla \Pi - \boldsymbol{\omega} \times \mathbf{u} + \nu \nabla^2 \mathbf{u}, \tag{1}$$

$$\nabla \cdot \mathbf{u} = 0, \tag{2}$$

where $\Pi = p/\rho - (\mathbf{\Omega} \times \mathbf{r}) \cdot (\mathbf{\Omega} \times \mathbf{r})/2 + \mathbf{u} \cdot \mathbf{u}/2$ and t is time. $\mathbf{u}$, $\boldsymbol{\omega}$, $\mathbf{\Omega}$, and $\mathbf{r}$ are vectors of velocity, vorticity, rotation rate, and position, respectively, ρ, p, and ν are density, pressure, and kinetic viscosity, respectively. Applying the Fourier transform with the continuity condition, the Navier–Stokes equations in wave space can be derived from Eq. (1),

$$\left(\frac{\partial}{\partial t} + \nu k^2 \right) \hat{\mathbf{u}}(\mathbf{k}) + \frac{2\mathbf{\Omega} \cdot \mathbf{k}}{k^2} [\mathbf{k} \times \hat{\mathbf{u}}(\mathbf{k})]$$

$$= -\sum_{\mathbf{k}-\mathbf{p}-\mathbf{q}=0} \left(1 - \frac{\mathbf{k}}{k^2} \mathbf{k} \cdot \right) [\hat{\boldsymbol{\omega}}(\mathbf{p}) \times \hat{\mathbf{u}}(\mathbf{q})]. \tag{3}$$

Here $\mathbf{k}$, $\mathbf{p}$, and $\mathbf{q}$ are the wave number vectors and $k^2 = \mathbf{k} \cdot \mathbf{k}$. An overcaret ^ denotes the Fourier transform. The second term on the left-hand side is the Coriolis term. The solenoidal condition implies that the velocity vector $\hat{\mathbf{u}}(\mathbf{k})$ is located on the plane normal to the wave number vector $\mathbf{k}$. The following decomposition for the velocity vector $\hat{\mathbf{u}}(\mathbf{k})$ is useful:

$$\hat{\mathbf{u}}(\mathbf{k}) = \xi_{+1} \mathbf{N}(\mathbf{k}) + \xi_{-1} \mathbf{N}(-\mathbf{k}) = \sum_{s=\pm 1} \xi_s \mathbf{N}(s\mathbf{k}). \tag{4}$$

This is the so-called "complex helical waves decomposition" (Lesieur,[14] Waleffe,[15] and Cambon[13]), and in this paper, it is used to analyze the effect of the Coriolis term on turbulence. The orthogonal basis $\mathbf{N}(s\mathbf{k})$ is defined as $\mathbf{N}(s\mathbf{k}) = \mathbf{e}^2(\mathbf{k}) - Is\mathbf{e}^1(\mathbf{k})$. The components ξ_{+1} and ξ_{-1} are the plus and minus helical modes, respectively. Here $\mathbf{k}$, $\mathbf{e}^1 = \mathbf{k} \times \mathbf{a}/|\mathbf{k} \times \mathbf{a}|$ and $\mathbf{e}^2 = \mathbf{k} \times \mathbf{e}^1/|\mathbf{k} \times \mathbf{e}^1|$ form a direct orthonormal frame called the Craya–Herring frame (Herring[16]), where $\mathbf{a}$ is an arbitrary constant vector. In this paper, we set $\mathbf{a} = (0,0,1)$. Then, the components of $\mathbf{N}(s\mathbf{k})$ are given by

$$\mathbf{N}(s\mathbf{k}) = \frac{1}{k\sqrt{k_1^2 + k_2^2}} [k_1 k_3 - Iskk_2, k_2 k_3 + Iskk_1,$$

$$- (k_1^2 + k_2^2)]^T, \tag{5}$$

where the superscript T denotes a transposed operator. Substituting the complex helical waves decomposition into Eq. (3), the evolution equations of the helical modes read as

$$\left(\frac{\partial}{\partial t} + \nu k^2 \right) \xi_{s_k} = \sum_{\mathbf{k}+\mathbf{p}+\mathbf{q}=0} \sum_{s_p, s_q} (s_p p - s_q q) g^* \xi_{s_p}^* \xi_{s_q}^*$$

$$+ Is_k g_k \xi_{s_k}. \tag{6}$$

The right-hand side has been written in a symmetric form in $\mathbf{p}$ and $\mathbf{q}$. Here $g^* = -(\mathbf{N}_{s_p}^* \times \mathbf{N}_{s_q}^* \cdot \mathbf{N}_{s_k}^*)/4$ is a geometrical factor depending on the shape and the orientation of the triad $(\mathbf{k}, \mathbf{p}, \mathbf{q})$, which satisfies the condition $\mathbf{k} + \mathbf{p} + \mathbf{q} = 0$. The triplet (s_k, s_p, s_q) is $(\pm 1, \pm 1, \pm 1)$ and $g_k = 2\Omega \cos \theta$, where θ is the angle between $\mathbf{k}$ and $\mathbf{\Omega}$. Since the k_3 axis is set as the rotation axis, θ is also equivalent to the azimuthal angle of the spherical coordinates.

III. LINEAR SOLUTION OF ANISOTROPY TENSOR

A. Linear solution of spectral tensor

Using the complex helical waves decomposition, the general form of the second-order spectral tensor is given by

$$\hat{U}_{ij}(\mathbf{k}) = \langle \hat{u}_i^* \hat{u}_j \rangle = e(\mathbf{k}) P_{ij}(\mathbf{k}) + \mathrm{Re}[Z(\mathbf{k}) N_i(\mathbf{k}) N_j(\mathbf{k})]$$

$$+ I\varepsilon_{ijl} k_l h(\mathbf{k})/k^2, \tag{7}$$

where $\langle \rangle$ denotes the ensemble average and $P_{ij}(\mathbf{k}) = \delta_{ij} - k_i k_j/k^2$ is the classic solenoidal projector. δ_{ij} and ε_{ijl} are the Kronecker delta and the alternation tensor, respectively. Here e, h, and Z are spectrums of energy, helicity, and complex deviator, respectively, defined by

$$e(\mathbf{k}) = \frac{1}{2} \langle \hat{\mathbf{u}}(\mathbf{k}) \cdot \hat{\mathbf{u}}^*(\mathbf{k}) \rangle = \sum_{s=\pm 1} \langle \xi_s(\mathbf{k}) \xi_s^*(\mathbf{k}) \rangle,$$

$$h(\mathbf{k}) = \frac{1}{2} \langle \hat{\mathbf{u}}(\mathbf{k}) \cdot \hat{\boldsymbol{\omega}}^*(\mathbf{k}) \rangle = k \sum_{s=\pm 1} \langle s\xi_s(\mathbf{k}) \xi_s^*(\mathbf{k}) \rangle, \tag{8}$$

$$Z(\mathbf{k}) = 2\langle \xi_{+1}(\mathbf{k}) \xi_{-1}^*(\mathbf{k}) \rangle.$$

One should note that Eq. (7) is valid for any anisotropic flow, not only axisymmetric without mirror symmetry. In physical space, the turbulence kinetic energy and helicity are defined by $\langle \mathbf{u} \cdot \mathbf{u} \rangle/2$ and $\langle \mathbf{u} \cdot \boldsymbol{\omega} \rangle/2$, respectively. The complex deviator is only defined in wave space, and it represents a part of the

Reynolds stress anisotropy in physical space. The corresponding governing equations of e, h, and Z can be derived from Eqs. (6) and (8),

$$\left(\frac{\partial}{\partial t} + 2\nu k^2\right) e(\mathbf{k}) = T^e(\mathbf{k}),$$

$$\left(\frac{\partial}{\partial t} + 2\nu k^2\right) h(\mathbf{k}) = T^h(\mathbf{k}), \qquad (9)$$

$$\left(\frac{\partial}{\partial t} + 2\nu k^2 - I4\Omega \cos\theta\right) Z(\mathbf{k}) = T^z(\mathbf{k}).$$

The right-hand sides are the transfer functions of e, h, and Z, respectively, corresponding to the nonlinear correlations of the turbulent velocity. Cambon et al.[10] numerically solved the system of equations (9) by closing with an isotropic EDQNM procedure accounting for resonant and nonresonant interactions (EDQNM2). The linear solutions of e, h, and Z are obtained by omitting the right-hand sides of the system equations:

$$e(\mathbf{k},t) = e(\mathbf{k},0)e^{-2\nu k^2 t},$$

$$h(\mathbf{k},t) = h(\mathbf{k},0)e^{-2\nu k^2 t}, \qquad (10)$$

$$Z(\mathbf{k},t) = Z(\mathbf{k},0)e^{-2\nu k^2 t}e^{I4\Omega t \cos\theta}.$$

In this paper, we introduce two parameters for further analysis. One is the phase difference $\phi_0(\mathbf{k})$ between the two complex helical modes, i.e., $\xi_{-1} = \gamma\xi_{+1}e^{-I\phi_0}$, where γ is the ratio of the moduli $|\xi_{-1}|/|\xi_{+1}|$. The other is a relative helicity coefficient, $\alpha(\mathbf{k})$, defined by

$$\alpha(\mathbf{k}) = \frac{h(\mathbf{k})}{ke(\mathbf{k})} = \frac{\langle \xi_{+1}\xi_{+1}^* - \xi_{-1}\xi_{-1}^* \rangle}{\langle \xi_{+1}\xi_{+1}^* + \xi_{-1}\xi_{-1}^* \rangle}. \qquad (11)$$

The definitions of $e(\mathbf{k})$ and $h(\mathbf{k})$ in Eq. (8) show that $\alpha = +1$ and -1 correspond to a turbulent field with the maximum and the minimum helicity, i.e., the Beltrami field, and $\alpha = 0$ corresponds to a turbulent field without helicity. Using these two parameters, the helicity and complex deviator spectrums can be expressed in terms of the energy spectrum $e(\mathbf{k},0)$ as

$$h(\mathbf{k},t) = e(\mathbf{k},0)e^{-2\nu k^2 t}k\alpha(\mathbf{k}),$$

$$Z(\mathbf{k},t) = e(\mathbf{k},0)e^{-2\nu k^2 t}\sqrt{1-\alpha(\mathbf{k})^2}e^{I[\phi_0(\mathbf{k})+4\Omega t \cos\theta]}. \qquad (12)$$

The general spectral tensor is then brought into the following form:

$$\hat{U}_{ij}(\mathbf{k},t) = e(\mathbf{k},0)e^{-2\nu k^2 t}\{P_{ij}(\mathbf{k}) + \sqrt{1-\alpha(\mathbf{k})^2}$$

$$\times \text{Re}[e^{I[\phi_0(\mathbf{k})+4\Omega t \cos\theta]}N_i(\mathbf{k})N_j(\mathbf{k})]$$

$$+ I\alpha(\mathbf{k})\varepsilon_{ijl}k_l/k\}. \qquad (13)$$

It is the general form of the linear solution for the second-order spectral tensor. For convenience, we only consider the turbulence without helicity and omit the viscosity, i.e., $\nu = 0$ and $\alpha = 0$. This simplification yields

$$\hat{U}_{ij}(\mathbf{k},t) = e(\mathbf{k},0)\{P_{ij}(\mathbf{k})$$

$$+ \text{Re}[e^{I[\phi_0(\mathbf{k})+4\Omega t \cos\theta]}N_i(\mathbf{k})N_j(\mathbf{k})]\}. \qquad (14)$$

Kassinos and Reynolds[11] showed an equivalent form of Eq. (14) by using the rapid distortion theory (RDT) in the investigation of the model for rotating homogeneous turbulence.

B. Formulation for anisotropy tensor

The Reynolds stress tensor and its anisotropy tensor are, respectively, defined by

$$R_{ij} = \langle u_i(\mathbf{x})u_j(\mathbf{x}) \rangle = \int \text{Re}[\hat{U}_{ij}(\mathbf{k})]d\mathbf{k}, \qquad (15)$$

$$b_{ij} = R_{ij}/q^2 - \delta_{ij}/3, \qquad (16)$$

where $q^2 = R_{ii} = 2\int e(\mathbf{k})d\mathbf{k}$. Using the general form of $\hat{U}_{ij}$, the anisotropy tensor of the Reynolds stress can be split into two parts, $b_{ij} = b_{ij}^e + b_{ij}^z$, with

$$b_{ij}^e = \int [e(\mathbf{k}) - e(k)]P_{ij}(\mathbf{k})d\mathbf{k}/q^2, \qquad (17)$$

$$b_{ij}^z = \int \text{Re}[Z(\mathbf{k})N_i(\mathbf{k})N_j(\mathbf{k})]d\mathbf{k}/q^2, \qquad (18)$$

where $e(k) = \int e(\mathbf{k})dA(k)/4\pi k^2$ is the shell-averaged spectrum and $\int(\ )dA(k)$ denotes integration on the shell with radius $k = |\mathbf{k}|$. Obviously, b_{ij}^e characterizes the departure of $e(\mathbf{k})$ from the shell-averaged spectrum $e(k)$, and it only exists when the distribution of $e(\mathbf{k})$ depends both on the magnitude and the direction (azimuthal angle θ of the spherical coordinates) of the wave number vector. Hence, b_{ij}^e is called the "directional anisotropy" in some reports (Cambon et al.[10] and Cambon and Jacquin[13]). On the other hand, b_{ij}^z denotes the departure of the spectral tensor from an isotropic distribution on the plane perpendicular to the wave number vector, and is called the "polarization anisotropy" (Cambon and Jacquin[13]).

It is beneficial here to repeat some theoretical statements of Kassinos and Reynolds[11] on homogeneous rotating turbulence before discussing the anisotropic behavior of the Reynolds stress tensor. They argued that the Reynolds stress tensor only is not sufficient to describe a homogeneous turbulence with system rotation, since the Reynolds stress does not have key information about the dimensionality of the turbulence structure, although it carries information about the turbulence components. Therefore, two new second-order tensors, the structure dimensionality (D_{ij}) and the structure circulicity (F_{ij}), are introduced into their study on turbulence modeling. D_{ij} and F_{ij} are defined by

$$D_{ij} = \left\langle \frac{\partial\psi_n}{\partial x_i}\frac{\partial\psi_n}{\partial x_j} \right\rangle, \quad F_{ij} = \left\langle \frac{\partial\psi_i}{\partial x_n}\frac{\partial\psi_j}{\partial x_n} \right\rangle, \qquad (19)$$

where ψ_i is the component of the vector potential corresponding to the fluctuation velocity. The velocity component is then given by $u_i = \varepsilon_{ist}\partial\psi_s/\partial x_t$. When the Fourier transforms of the vector potential and the velocity are used in Eq. (19), one obtains

Phys. Fluids, Vol. 13, No. 10, October 2001

Dynamics of anisotropy on decaying   2915

$$D_{ij}=2\int \frac{k_i k_j}{k^2} e(\mathbf{k})d\mathbf{k}=q^2\left(\frac{\delta_{ij}}{3}-2b_{ij}^e\right),$$
(20)

$$F_{ij}=\int \varepsilon_{inm}\varepsilon_{jts}\frac{k_n k_t}{k^2}\hat{U}_{ms}(\mathbf{k})d\mathbf{k}=q^2\left(\frac{\delta_{ij}}{3}+b_{ij}^e-b_{ij}^z\right).$$

Note that $D_{ii}=F_{ii}=R_{ii}=q^2$. The anisotropy tensors for D_{ij} and F_{ij} are, respectively, defined by

$$y_{ij}=D_{ij}/q^2-\delta_{ij}/3, \quad x_{ij}=F_{ij}/q^2-\delta_{ij}/3.$$
(21)

The relations between b_{ij}^e, b_{ij}^z, and y_{ij}, x_{ij} are then given by

$$b_{ij}^e=-y_{ij}/2, \quad b_{ij}^z=-(2x_{ij}+y_{ij})/2.$$
(22)

The continuity equation leads to $b_{ij}+y_{ij}+x_{ij}=0$. According to the theoretical statement of Kassinos and Reynolds,[11] y_{ij} and x_{ij} carry the structure information of turbulence, which is not included in b_{ij}. Equation (22) indicates that b_{ij}^e and b_{ij}^z also carry the structure information of turbulence. Hence, when two terms of set (b_{ij}, y_{ij}, x_{ij}) or set $(b_{ij}, b_{ij}^e, b_{ij}^z)$ are known, we know that there is enough information to describe a homogeneous turbulence subjected to system rotation.

Using the axisymmetric condition $e(\mathbf{k})=e(k,\theta)$ which is satisfied in a rotating system and the inviscid linear solution of the spectral tensor, the Reynolds stress can be further expressed in the following form:

$$R_{ij}(t)=q^2\frac{\delta_{ij}}{3}+\int [e(k,\theta)-e(k)]P_{ij}(\mathbf{k})d\mathbf{k}$$

$$+\int \mathrm{Re}[e(k,\theta)e^{I[\phi_0(\mathbf{k})+4\Omega t\cos\theta]}$$

$$\times N_i(\mathbf{k})N_j(\mathbf{k})]d\mathbf{k}.$$
(23)

Assuming that $e(k,\theta)=e(k)f(k,\theta)$, the directional anisotropy tensor b_{ij}^e is brought into the following form:

$$b_{ij}^e(t)=\frac{1}{q^2}\int e(k)P_{ij}(\mathbf{k})[f(k,\theta)-1]d\mathbf{k},$$
(24)

where $f(k,\theta)$ is a nondimensional distribution function. The polarization anisotropy b_{ij}^z can further be split into a linear part b_{ij}^{zl} and a nonlinear part b_{ij}^{zn}, where

$$b_{ij}^{zl}(t)=\frac{1}{q^2}\int e(k)\mathrm{Re}[e^{I[\phi_0(\mathbf{k})+4\Omega t\cos\theta]}N_i(\mathbf{k})N_j(\mathbf{k})]d\mathbf{k},$$
(25)

$$b_{ij}^{zn}(t)=\frac{1}{q^2}\int e(k)\mathrm{Re}[e^{I[\phi_0(\mathbf{k})+4\Omega t\cos\theta]}N_i(\mathbf{k})N_j(k)]$$

$$\times[f(k,\theta)-1]d\mathbf{k}.$$

Note that $P_{ij}(\mathbf{k})$ and $N_i(\mathbf{k})N_j(\mathbf{k})$ are geometric tensors and do not vary with rotation rate or time. Hence, the linear term $e^{I(\phi_0+4\Omega t\cos\theta)}$ and the distribution function $f(k,\theta)$ completely determine the evolutions of these anisotropy tensors. The DNS results in Sec. V show that $f(k,\theta)$ only varies with the coupling effect of the system rotation. Thus, b_{ij}^e mainly reflects the coupling effect of system rotation. On the other hand, b_{ij}^z mainly reflects the linear effect of the system rotation due to the strong linear effect from the term $e^{I(\phi_0+4\Omega t\cos\theta)}$, although the coupling effect also acts on the evolution of b_{ij}^{zn} through the term $f(k,\theta)-1$. Equations (24)

and (25) indicate that the linear solution of b_{ij}^e exists only with $f(k,\theta)\neq 1$, and the evolution of b_{ij}^z is influenced by the presence of b_{ij}^e.

C. Linear solution of anisotropy tensor

In the spherical coordinate system (k,θ,φ), the Reynolds stress tensor can be expressed as

$$R_{ij}(t)=\int_0^\infty \int_0^\pi \int_0^{2\pi} k^2\hat{U}_{ij}(\mathbf{k},t)\sin\theta d\varphi d\theta dk.$$
(26)

Mansour et al.[12] adopted a model for the spectral tensor $\hat{U}_{ij}$ proposed by Cambon et al.[17] and Shih et al.[18] and derived a linear solution of the anisotropy b_{ij} with one parameter and two undetermined functions. However, their linear solution of b_{ij} contains a number of coefficients, and the initial anisotropy does not relate to their model parameter. Here we present a simpler form for b_{ij} with only one parameter that determines the initial anisotropy of the homogeneous turbulence.

In the rotating frame, the spectral tensor $\hat{U}_{ij}$ satisfies not only the axisymmetric condition but also the reflectional symmetry about the equator plane with the real symmetry $\hat{U}_{ij}^*(\mathbf{k})=\hat{U}_{ij}(-\mathbf{k})$. Hence, Eq. (26) can be brought into the following form:

$$R_{ij}(t)=\int_0^\infty \int_0^{\pi/2} 4\pi k^2\hat{U}_{ij}(\mathbf{k},t)\sin\theta d\theta dk.$$
(27)

This equation then becomes integrable assuming a spherical distribution, $e(k,\theta)=e(k)$, i.e., $f(k,\theta)=1$ and $\phi_0(\mathbf{k})$ is a constant. The integral is

$$R_{ij}(t)=q^2(0)\left(\frac{\delta_{ij}}{3}+(\delta_{ij}-3\delta_{i3}\delta_{j3})b(\Omega t)\right),$$
(28)

with

$$b(\Omega t)=\frac{\cos\phi_0}{2}\left(\frac{\cos(4\Omega t)}{(4\Omega t)^2}-\frac{\sin(4\Omega t)}{(4\Omega t)^3}\right)$$

$$-\frac{\sin\phi_0}{2}\left(\frac{\sin(4\Omega t)}{(4\Omega t)^2}+\frac{\cos(4\Omega t)-1}{(4\Omega t)^3}-\frac{1}{8\Omega t}\right).$$
(29)

Equation (28) is the linear solution of the Reynolds stress tensor for the inviscid rotating homogeneous turbulence. The corresponding linear solution of the anisotropy tensor is given by

$$b_{ij}^e(t)=b_{ij}^e(0)=0,$$

$$b_{ij}^{zn}(t)=b_{ij}^{zn}(0)=0,$$
(30)

$$b_{ij}(t)=b_{ij}^{zl}(t)=(\delta_{ij}-3\delta_{i3}\delta_{j3})b(\Omega t).$$

Since

$$\lim_{\Omega t\to 0} b_{ij}(t)=-(\delta_{ij}-3\delta_{i3}\delta_{j3})\cos\phi_0/6,$$
(31)

TABLE I. Initial states of a turbulent field.

α	ϕ_0	$e(\mathbf{k})$	$h(\mathbf{k})$	$\mathrm{Re}[Z(\mathbf{k})]$	$\mathrm{Im}[Z(\mathbf{k})]$	$b_{ij}=b^z_{ij}$			State
α	ϕ_0	$e(\mathbf{k})$	$\alpha k e(\mathbf{k})$	$|Z|\langle \cos\phi_0\rangle$	$|Z|\langle \sin\phi_0\rangle$	b_{11}	b_{22}	b_{33}	
1	Arbitrary	$e(\mathbf{k})$	$ke(\mathbf{k})$	0	0	0	0	0	Isotropic
	Random	$e(\mathbf{k})$	0	0	0	0	0	0	Isotropic
0	0°	$e(\mathbf{k})$	0	$e(\mathbf{k})$	0	$-1/6$	$-1/6$	$1/3$	Anisotropic
	90°			0	$e(\mathbf{k})$	0	0	0	Isotropic
	180°			$-e(\mathbf{k})$	0	$1/6$	$1/6$	$-1/3$	Anisotropic
	270°			0	$-e(\mathbf{k})$	0	0	0	Isotropic

the initial anisotropy is determined completely by the single parameter, ϕ_0. In addition, it is verified that the assumption of $f(k,\theta)=1$ is reasonable by comparing the linear solution with the DNS results.

IV. GENERATION OF INITIAL ANISOTROPY

First, a precomputation is carried out until a time $t_0 = 2.5$ (s) to obtain a numerically isotropic turbulent field. The velocity gradient skewness is about -0.5 at this time, showing that the nonlinear correlation of the turbulence is built completely (Orszag and Patterson[19]). The helical modes of this initially isotropic turbulent field can be expressed simply as

$$\xi^0_{+1}(\mathbf{k},t_0)=|\xi^0_{+1}(\mathbf{k},t_0)|\exp(I\phi_{+1}),$$
$$\xi^0_{-1}(\mathbf{k},t_0)=|\xi^0_{-1}(\mathbf{k},t_0)|\exp(I\phi_{-1}),$$
(32)

where ϕ_{+1} and ϕ_{-1} are the phases of ξ^0_{+1} and ξ^0_{-1}, respectively. In order to submit the DNS of rotating turbulence with or without the initial anisotropy, we propose a numerical method to introduce the polarization anisotropy into the isotropic turbulent field. Using the phase difference ϕ_0 and the relative coefficient of helicity α, Eq. (32) becomes

$$\xi_{+1}(\mathbf{k},t_0)=\sqrt{\frac{(1+\alpha)e^0}{2}}\exp[I\phi_{+1}],$$
$$\xi_{-1}(\mathbf{k},t_0)=\sqrt{\frac{(1-\alpha)e^0}{2}}\exp[I(\phi_{+1}-\phi_0)],$$
(33)

where $e^0=|\xi^0_{+1}|^2+|\xi^0_{-1}|^2$ is the kinetic energy of the isotropic turbulence at t_0. The states of the turbulent field are shown in Table I, corresponding to different values of ϕ_0 and α. Table I shows that the turbulence remains isotropic ($|z|=0$) when ϕ_0 is randomly distributed in wave space. With a constant distribution of ϕ_0, Eq. (33) introduces the complex deviator ($|Z|\neq0$) into the turbulence. However, one can find from Table I that only the real part of the complex deviator introduces the polarization anisotropy into the system, while the imaginary part cannot change the anisotropy of the initially isotropic homogeneous turbulence.

In addition, Eq. (33) also effectively introduces helicity into the turbulent field. Polifke and Shtilman[20] used a random phase method to introduce the helicity into the field, based on the definition of the helicity spectrum. However, it needs many complex procedures to obtain an effective field with only small helicity. When ϕ_0 in Eq. (33) has a random

distribution, one can introduce the helicity into the turbulent field simply with parameter α only, which determines the intensity of the helicity. Using a similar method to introduce the initial helicity into the turbulent field, Morinishi et al.[21] investigated the helicity effects on the rotating turbulence in detail.

V. DNS RESULTS AND DISCUSSION

In this paper, we simulate the homogeneous decaying turbulence subjected to system rotation using DNS with a pseudospectral method. The Coriolis and viscous terms in the N–S equations are treated using an integrating factor technique to integrate them analytically. With using the complex helical waves decomposition, Yeung and Zhou[22] and Smith and Waleffe[23] used a similar technique to simulate forcing turbulence. The numerical stability analysis and detailed scheme for this technique are introduced in Ref. 24. The other terms in the N–S equations are integrated by a fourth-order Runge–Kutta explicit method. The simulation domain is a $(2\pi)^3$ periodic box, and the spectral mode number is set to 128 in each direction. The kinetic viscosity and the time increment are $\nu=0.01$ (m²/s) and $\Delta t=0.01$ (s), respectively. Some of the statistics of the initial field are presented in Table II. Here, K_0 (m²/s²), ε_0 (m²/s³), Re_λ and S are kinetic energy, energy dissipation rate, Reynolds number based on the Taylor microscale, and the skewness factor of $(-\partial u_1/\partial x_1)$ at the initial time. Two sets of simulation (sets A and B) are performed in this study. Set A is the DNS of homogeneous turbulence with the initial polarization anisotropy. The results are used to verify the linear solution of the anisotropy with $\Omega=0,10$ (rad/s), corresponding to Table I. Set B is the DNS of homogeneous turbulence without the initial polarization anisotropy, and its results are used to investigate the coupling effect on the anisotropy with a series of rotation rates. All the simulations are carried out without the initial helicity ($\alpha=0$).

TABLE II. Statistics of an initial turbulent field at $t_0=2.5$ (s).

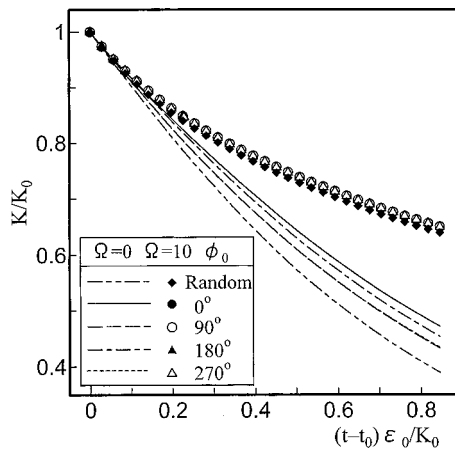| K_0	ε_0	Re_λ	S
0.201 26	0.0567	53.4	0.4960

FIG. 1. Evolution of kinetic energy.

FIG. 3. Evolution of b_{ij} (DNS results).

A. Linear effect of system rotation on anisotropy tensor

In this subsection, the DNS results of set A are used for the following discussion. The time evolution of the nondimensional kinetic energy is shown in Fig. 1, where the abscissa is the lapse time nondimensionalized by ε_0/K_0. As demonstrated in many studies (e.g., Jacquin et al.,[1] Morinishi et al.,[24] and Squires et al.[25]), decay of the kinetic energy is inhibited by the system rotation. It is also inhibited by the presence of the initial polarization anisotropy (in cases $\phi_0 = 0°$ and 180°) in the stationary frame. In a strong rotating system, this inhibition effect of the initial polarization anisotropy is small. However, even in the initially isotropic cases of $\phi_0 = 90°$ and 270°, the decay of the kinetic energy in the stationary frame is slower than that when $\phi_0 = $ random. It can be considered to be the effect of the phase disturbance when a certain value of the phase difference ϕ_0 is introduced into the turbulent field. The phase disturbance destroys the nonlinear interactions of the turbulence (Murakami et al.[26]) and leads to a weakened energy transfer by the same mechanism as that of the system rotation.

Figure 2 shows the anisotropy invariant map (AIM) of the Reynolds stresses. II_b and III_b are the second and third
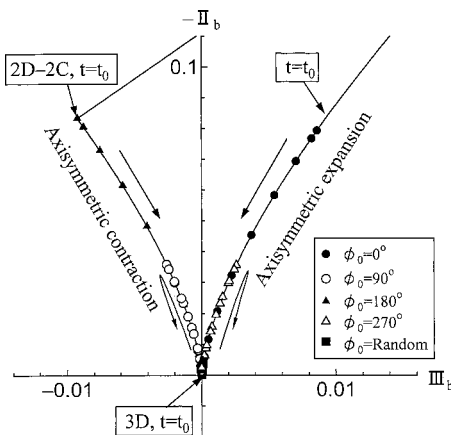
invariants of the anisotropy tensor b_{ij}, respectively, defined by

$$II_b = -b_{ij}b_{ji}/2, \quad III_b = -b_{ij}b_{jk}b_{ki}/3. \quad (34)$$

The figure shows that the cases $\phi_0 = 0°$ and 180°, corresponding to the axisymmetric expansion (AXE) and contraction (AXC) states (Kassinos and Reynolds[11]), approach the origin (isotropic state) with the time evolution. In the cases $\phi_0 = 90°$ and 270°, although their states are initially isotropic, the values of $-II_b$ increase with the time evolution along the limit line of AXC and AXE, and return to the origin again in a later stage of their evolution. The evolution of anisotropy is shown more quantitatively in the next figures. Figure 3 shows the DNS result for the evolution of b_{ij}. Only b_{33} is shown in the figure since $b_{33} = -2b_{11} = -2b_{22}$ when the rotating or axisymmetric flow is considered. In the cases of $\phi_0 = 0°$ and 180°, the anisotropy in the stationary frame decays gradually due to the viscosity, while in the rotating system it decreases rapidly to a nearly isotropic state within about one period of its oscillation. In the initially isotropic cases of $\phi_0 = 90°$ and 270°, b_{33} evolves with little variation in the stationary frame. While in the rotating system, it shows a "pulse" at the initial period of the evolution and then returns to zero with a slight oscillation. It corresponds to the behavior of its invariants in Fig. 2. These DNS
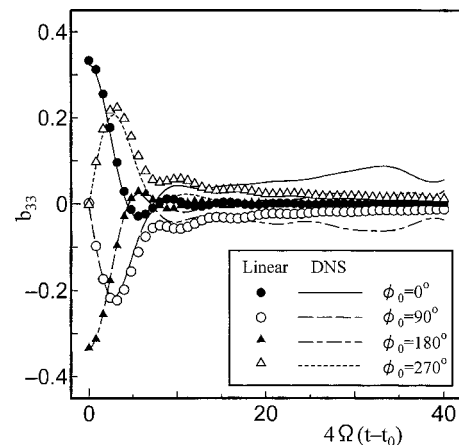

FIG. 2. Anisotropy invariant map (AIM) of Reynolds stresses.

FIG. 4. A comparison between DNS results and a linear solution of b_{ij}.
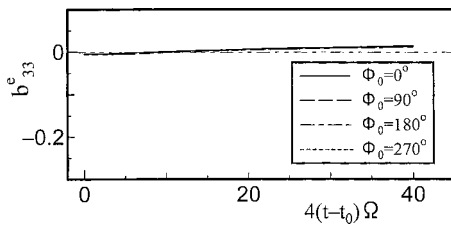
FIG. 5. Evolution of directional anisotropy.

FIG. 7. Evolution of kinetic energy.

results are well described by the linear solution of the anisotropy tensor, at least in the first period of evolution. Figure 4 shows a comparison between the DNS results of $b_{ij}(b_{ij}^e + b_{ij}^{zn} + b_{ij}^{zl})$ and the linear solutions (b_{ij}^{zl} only). It shows that the linear solutions agree very well with the DNS results in the first period of the evolution. Hence, at least in the first period of the evolution of b_{ij}^z, one can say that the linear effect of the system rotation is dominant. The evolutions of b_{ij}^e and b_{ij}^{zn} are shown in Figs. 5 and 6, respectively. Although the linear solutions of b_{ij}^e and b_{ij}^{zn} are zero because $f(k,\theta)=1$, the DNS results of b_{ij}^e and b_{ij}^{zn} are generated due to the nonlinearity, showing that the distribution function $f(k,\theta)$ is changed by the coupling effect. The evolution of b_{ij}^{zn} also takes on some oscillations. However, compared with the initial values of b_{ij}^{zl}, the values of b_{ij}^e and b_{ij}^{zn} are small. As shown in Fig. 5, the evolution of b_{ij}^e does not depend on the presence of the initial polarization anisotropy. A more detailed discussion about b_{ij}^e is given in the next section. Since b_{ij}^{zl} can be estimated by the inviscid linear solution, the value of b_{ij}^{zn} ($b_{ij}^{zn}=b_{ij}-b_{ij}^e-b_{ij}^{zl}$) in Fig. 6 is a little different from the real value of b_{ij}^{zn}, which includes the effect of viscosity.

B. Coupling effect on anisotropy tensor

The above analysis shows that the linear effect of the system rotation does not act on the evolution of the directional anisotropy b_{ij}^e. The coupling effect on the energy spectrum $e(k,\theta)$ and behavior of b_{ij}^e are investigated here using the DNS results of set B.

Some of the properties of the coupling effect are presented here first. The evolution of the kinetic energy is shown in Fig. 7, where the symbol $\triangle$ denotes the numerical solutions of the Stokes equations (omitting the convective term in the N–S equations). The figure shows that the decaying behavior of the kinetic energy in a strong rotating frame
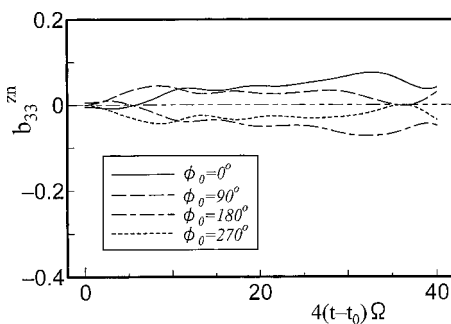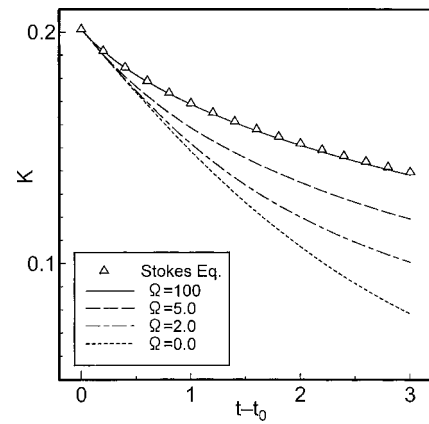
[e.g., $\Omega=100\,(\text{rad/s})$] is almost the same as that of the Stokes equations. Obviously, the decaying behavior according to the Stokes equations does not depend on the system rotation. Hence, the differences between the solutions of the N–S and the Stokes equations for each rotation rate indicate the effect of the nonlinear interaction. The nonlinear interaction decreases with increasing rotation rates, so the effect of the nonlinear interaction is inhibited by the rotation.

The energy spectrums $e(k,\theta)$ with $\Omega=0$, 5 and 100 (rad/s) are presented in Figs. 8(a), 8(b), and 8(c), respectively. In the stationary frame, the value of the energy spectrum decreases with increasing wave number k and does not depend on the azimuthal angle θ. Therefore, an isotropic distribution of the energy spectrum on the shell with radius k can be imaged. At the intermediate rotation range, the value of the energy spectrum decreases with increasing k at θ = const, and decreases with increasing $\cos\theta$ at k = const. Hence, the value of $e(k,\theta)$ near the equator ($\cos\theta=0$) is larger than that near the pole ($\cos\theta=1$). Although $e(k,\theta)$ still exhibits a decreasing behavior with θ in high wave number regions, the distribution of $e(k,\theta)$ approaches an isotropic distribution again when the system rotation becomes very strong, when we compare the scale of Fig. 8(c) with Fig. 8(b). In this case, the coupling effect is negligible because the nonlinear interaction is inhibited by the strong rotation. Consequently, only when the coupling effect is dominant, i.e., both the nonlinear interaction and the Coriolis force have a certain value, does the energy spectrum take on an anisotropic distribution. The deviation of $e(k,\theta)$ from an isotropic one can be considered an indicator of the level of the coupling effect, which then closely related to the directional anisotropy b_{ij}^e, as shown in Eq. (24).

The time evolutions of b_{33}^e are shown in Figs. 9(a) and 9(b). In the rotating system, b_{33}^e increases with time, although its initial value is almost zero. In the stationary frame, b_{33}^e does not vary with time due to the lack of the coupling effect. Here b_{33}^e increases with the increase in the rotation rate for $0 \le \Omega \le 2.51$ (rad/s), and the increasing rate of b_{33}^e decreases when the rotation rate is further increased [$\Omega > 2.51$ (rad/s)]. The evolution of b_{33}^e for $\Omega = 100$ (rad/s) is almost the same as that for $\Omega = 0$, since the coupling effect becomes negligibly small in this case. Then, we can say that
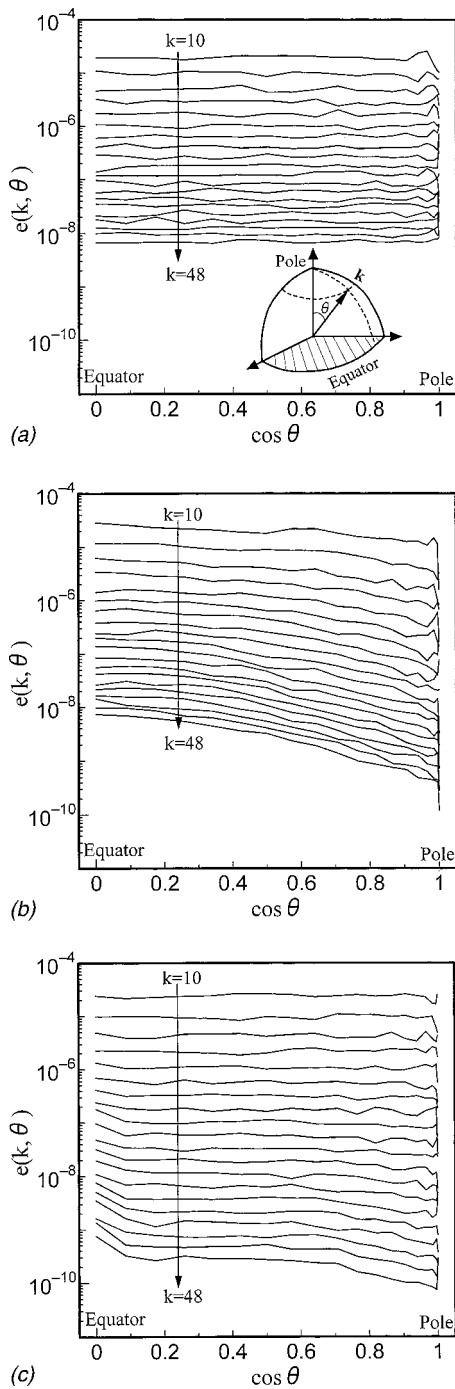

FIG. 6. Evolution of the nonlinear part of polarization anisotropy.

FIG. 8. Distribution of the energy spectrum at $t-t_0=1$ (s). (a) $\Omega=0$ (rad/s); (b) $\Omega=5$ (rad/s); (c) $\Omega=100$ (rad/s).
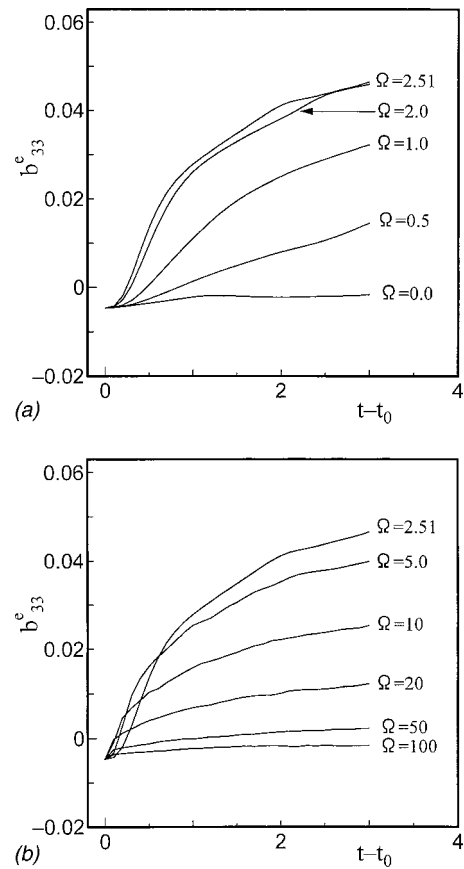

FIG. 9. The evolution of directional anisotropy. (a) Low rotation rate; (b) high rotation rate.

$$\mathrm{Ro}^L=u'/(2\Omega L), \quad \mathrm{Ro}^\lambda=u'/(2\Omega\lambda),$$
$$\mathrm{Ro}^\omega=\omega'/(2\Omega)=\sqrt{15}\mathrm{Ro}^\lambda. \tag{35}$$

Here $L=u'K/\varepsilon$ and $\lambda=\sqrt{15}u'/\omega'$ denote a typical length scale and Taylor microscale, respectively, where u' and ω' are rms velocity and vorticity fluctuations, and ε is the dissipation rate of the kinetic energy. Figure 10 shows that b_{33}^e and b_{33}^z are both produced by the system rotation and contribute oppositely to the evolution of b_{33}. The value of b_{33}^e varies with the rotation rate and reaches a peak value at
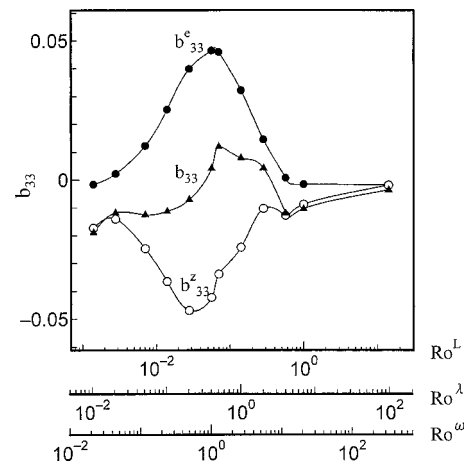
the directional anisotropy b_{33}^e directly reflects the level of the coupling effect.

Jacquin et al.[1] showed the fact that the range of Rossby number for anisotropization effects has an upper and a lower limit by looking at the integral length scale through their experimental results. Here we show the limits of the Rossby number for the anisotropy b_{33}, b_{33}^e, and b_{33}^z in Fig. 10 at $t-t_0=3$ (s) against the initial Rossby numbers (at $t=t_0$). The macro-Rossby number Ro^L, and micro-Rossby numbers Ro^λ and Ro^ω, are defined by

FIG. 10. The variation of anisotropy with Rossby numbers.
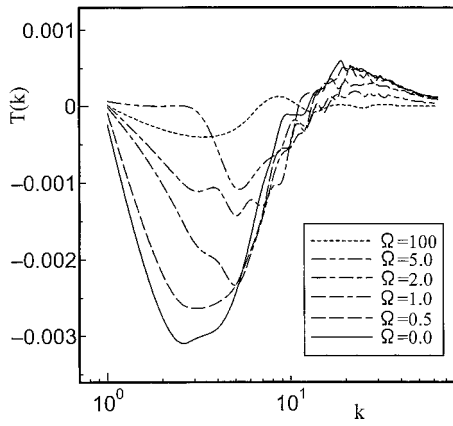
FIG. 11. The variation of an energy transfer function with the rotation rate.

FIG. 12. The variation of forward and reverse cascades with a rotation rate $[p,q \geq k,\ t-t_0=1\ (\text{s})]$.

about $\text{Ro}^{\lambda} \cong 0.4$, corresponding to the maximum coupling effect. In this paper, one can find that the anisotropy and the two-dimensionalization are excited at a range of $\text{Ro}^{L}<1$ and $\text{Ro}^{\lambda}>0.01$, which is larger than the intermediate range of $\text{Ro}^{L}<1$ and $\text{Ro}^{\lambda}>1$ introduced by Cambon et al.[10]

C. Direction of local energy transfer

The effects of the system rotation on the local energy transfer between the pole and the equator are investigated in this section to understand why the energy spectrum departs from an isotropic one.
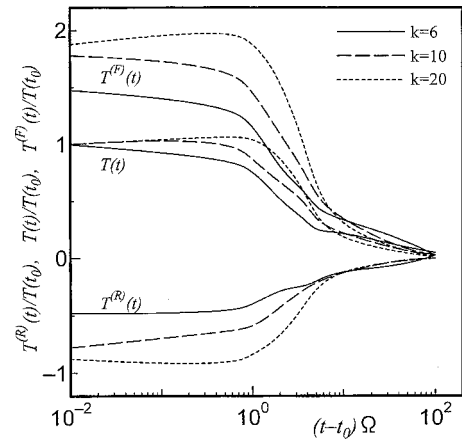
Figure 11 shows the profiles of the energy transfer function of rotating turbulence. The absolute value of the energy transfer function decreases with an increasing rotation rate. The higher the rotation rate, the smaller the absolute value of the energy transfer function. When $\Omega=100\ (\text{rad/s})$, the energy transfer from the low to high wave number becomes nearly zero. As with the decay of the kinetic energy, the energy transfer is also inhibited by the system rotation. These phenomena are usually demonstrated by the so-called "scrambling effect" of the system rotation. However, the scrambling effect provides no information about the direction of the energy transfer.

Using the helical modes, one finds that the energy transfer function can be expressed as

$$T(\mathbf{k})=\sum_{\mathbf{k}+\mathbf{p}+\mathbf{q}=0}\sum_{s_k,s_p,s_q} 2(s_p p - s_q q)$$
$$\times \text{Re}\langle g^* \xi_{s_k}^*(\mathbf{k}) \xi_{s_p}^*(\mathbf{p}) \xi_{s_q}^*(\mathbf{q})\rangle. \tag{36}$$

From this expression, one knows that the kinetic energy transfer is a sum of all detailed triad interactions $\langle \xi_{s_k} \xi_{s_p} \xi_{s_q}\rangle$. There are two helical modes for a wave number vector, so eight possible interactions numbered from 0 to 7 following a binary order are allowed in the triad $(\mathbf{k}, \mathbf{p}, \mathbf{q})$, which satisfies $\mathbf{k}+\mathbf{p}+\mathbf{q}=0$ according to the helical mode signs (s_k,s_p,s_q), i.e.,

$$0 \equiv (+,+,+), \quad 1 \equiv (+,+,-), \quad 2 \equiv (+,-,+),$$
$$3 \equiv (+,-,-), \quad 4 \equiv (-,+,+), \quad 5 \equiv (-,-,+), \tag{37}$$
$$6 \equiv (-,+,-), \quad 7 \equiv (-,-,-).$$

Waleffe[15,27] used the "instability assumption" to evaluate the direction of the energy transfer. He classifies these interactions into two types: the "forward" and the "reverse" interactions with their wave number scales (k, p, q) and helical mode signs (s_k,s_p,s_q). A forward interaction transfers the energy from a low to a high wave number, while a reverse interaction transfers the energy from a high to a low wave number. According to the instability assumption,[15] when the wave numbers of the triad $(\mathbf{k}, \mathbf{p}, \mathbf{q})$ are given as $k<p\leq q$, the triad interactions 0, 3, 4, and 7 are "reverse" interactions, corresponding to a reverse cascade to the lowest wave number k; while the triad interactions 1, 2, 5, and 6 are "forward" interactions, corresponding to a forward cascade from k to higher wave numbers p and q. Now, the energy transfer function [Eq. (36)] can be brought into the following form:

$$T(\mathbf{k})=\sum_{i=0}^{7} T^{(i)}(\mathbf{k}),$$

$$T^{(i)}(\mathbf{k})=\sum_{\mathbf{k}+\mathbf{p}+\mathbf{q}=0} 2(s_p p - s_q q)$$

$$\times \text{Re}\langle g^* \xi_{s_k}^*(\mathbf{k}) \xi_{s_p}^*(\mathbf{p}) \xi_{s_q}^*(q)\rangle. \tag{38}$$

Then, a forward and a reverse cascade energy transfer functions, $T^{(F)}(t)$ and $T^{(R)}(t)$ are, respectively, defined, as

$$T^{(F)}(t)=\int [T^{(1)}(\mathbf{k},t)+T^{(2)}(\mathbf{k},t)+T^{(5)}(\mathbf{k},t)$$
$$+T^{(6)}(\mathbf{k},t)]dA(k), \tag{39a}$$

$$T^{(R)}(t)=\int [T^{(0)}(\mathbf{k},t)+T^{(3)}(\mathbf{k},t)+T^{(4)}(\mathbf{k},t)$$
$$+T^{(7)}(\mathbf{k},t)]dA(k). \tag{39b}$$

Figure 12 shows the variation of $T^{(F)}(t)$ and $T^{(R)}(t)$ with increase of the rotation rate at wave numbers $k=6$, 10, and 20, respectively. Here, $T(t)=T^{(F)}(t)+T^{(R)}(t)$ is the total energy transfer function. The figure shows that both the forward and the reverse cascades exist in the turbulence. The quantity of the forward cascade is always larger than that of the reverse one, and the total energy transfer only takes on a
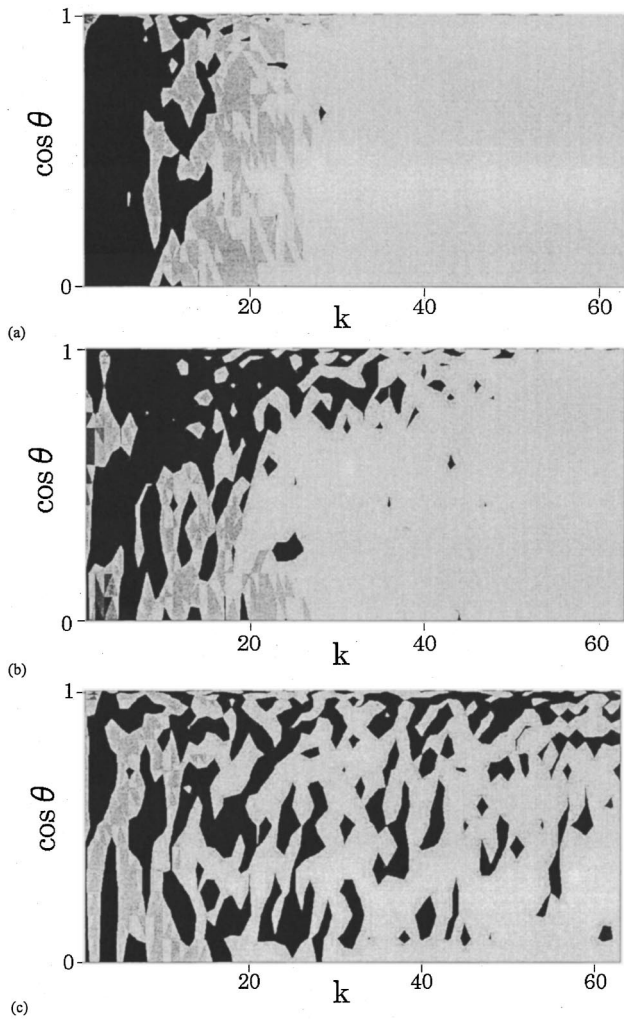
FIG. 13. Distribution of the energy transfer function at $t-t_0=1$ (s). (a) $\Omega=0$ (rad/s); (b) $\Omega=5$ (rad/s); (c) $\Omega=100$ (rad/s).

FIG. 14. Direction of the local energy transfer.

forward form. In addition, Fig. 12 also shows that the scrambling effect of the system rotation inhibits both the forward and reverse cascades, and the total effect is to decrease the total energy transfer to almost zero.

     Some of the properties of the energy transfer in the rotating turbulence can be seen in Fig. 13, which shows the distribution of the energy transfer function $T(k,\theta)$ with different rotation rates. The black region in Fig. 13 denotes the negative value of $T(k,\theta)$ and the other region is positive, where the deep gray region denotes a relatively large positive value. Hence, the kinetic energy is transferred from the black region to the other regions. The figure shows that, in the case of $\Omega=0$ (rad/s), a forward energy cascade from low to high wave number is dominant. On the other hand, when $\Omega=5$ (rad/s), the negative value enlarges its area near the pole. It means that the kinetic energy is transferred in the k and θ directions. The energy transfer in the direction of k is a cascade from low to high wave number, while the transfer in the direction of θ can be considered a local energy transfer from the pole to the equator on the shell with radius k. In cases of strong rotation, such as $\Omega=100$ (rad/s), the kinetic energy transfer function is randomly distributed in the $k-\theta$ plane,
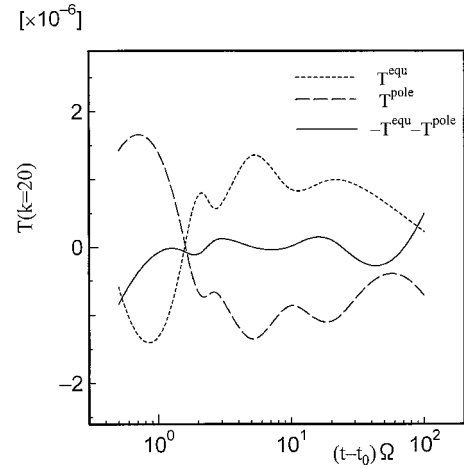
and the mean value of the energy transfer function approaches zero, as shown in Fig. 11. We can conclude from these results that the local energy transfer is caused by the coupling effect that mainly occurs in cases of moderate rotation, because no local energy transfer exists in both weak and strong rotation cases. Strong rotation inhibits not only the local energy transfer from the pole to the equator but also the cascade from low to high wave number. These two types of energy transfer directly induce different distributions of kinetic energy, as shown in Fig. 8. Morinishi et al.[24] verified the anisotropic distribution of the kinetic energy in a rotating system by providing the anisotropic velocity distributions in wave space.

     To provide some idea of the local energy transfer from the pole to equator, for example, we show in Fig. 14 the value of the energy transfer function on the shell with radius $k=20$. Here, T^{equ} denotes the energy transfer function near the equator of the shell with radius $k=\text{const}$, defined by

$$T^{\text{equ}}(t) = \sum_{\substack{\mathbf{k}+\mathbf{p}+\mathbf{q}=0 \\ 45^\circ \leqslant \theta \leqslant 135^\circ}} [-P_{ijm}(\mathbf{k})\text{Im}\langle \hat{u}_i(\mathbf{k})$$
$$\times \hat{u}_j(\mathbf{p})\hat{u}_m(\mathbf{q})\rangle]|_{k=p=|\mathbf{k}|=\text{const}}, \quad (40)$$

with $P_{ijm}=k_m P_{ij}+k_j P_{im}$, while T^{pole} denotes the energy transfer function near the pole of the shell with radius $k=\text{const}$,

$$T^{\text{pole}}(t) = T(t) - T^{\text{equ}}(t), \quad (41)$$

where

$$T(t) = \sum_{\mathbf{k}+\mathbf{p}+\mathbf{q}=0} [-P_{ijm}(\mathbf{k})\text{Im}\langle \hat{u}_i(\mathbf{k})$$
$$\times \hat{u}_j(\mathbf{p})\hat{u}_m(\mathbf{q})\rangle]|_{k=p=|\mathbf{k}|=\text{const}}. \quad (42)$$

Here, $-(T^{\text{equ}}+T^{\text{pole}})$, the rate of total energy transfer between $\mathbf{k}$ and the other wave numbers, is also plotted in the figure for considering the detailed conservation property of the energy transfer function. The figures show that the energy transfer to the other wave numbers $-(T^{\text{equ}}+T^{\text{pole}})$ is small, and almost all the energy transfer occurs between the pole and the equator. When $(t-t_0)\Omega$ increases to a certain

value, T^{equ} keeps a positive value and T^{pole} a negative value. Then, one can say that the kinetic energy of the rotating turbulence is locally transferred from the region near the pole toward the equator. From the above analysis, we found that the coupling effect causes a local energy transfer from the pole to the equator. Moreover, this local energy transfer introduces the anisotropic distribution of the energy spectrum $e(k, \theta)$ and then the anisotropy of the Reynolds stress tensor.

VI. CONCLUDING REMARKS

In this paper, the effect of the system rotation on the anisotropy of the Reynolds stresses is investigated by using theoretical analysis and DNS results. Based on the governing equations of the rotating turbulence and the complex helical wave decomposition, we derived a simple form of the linear solution of the anisotropy. In addition, the useful relationship between the anisotropic formalism developed by Cambon and co-workers and the one by Reynolds and co-workers was revealed. A numerical method to introduce the anisotropy into an initially isotropic turbulence is then proposed. Using this method, the DNS of homogeneous rotating turbulence with and without initial anisotropy is carried out to investigate the linear and coupling effects on the anisotropy.

Theoretical analysis shows that the anisotropy can be split into two parts: the polarization anisotropy and directional anisotropy, and the polarization anisotropy can further be separated into a pure linear part and a nonlinear part. As the linear solution of the (polarization) anisotropy agrees well with the DNS results for the initial evolution period, the linear effect of the system rotation determines the evolution of the polarization anisotropy. We found that the presence of the polarization anisotropy inhibits the decay of the kinetic energy in the stationary frame, while in the rotating system, the initial polarization anisotropy decays rapidly with the time scale $(t-t_0)\Omega$ and the inhibition effect becomes small. With a moderate rotation rate, the coupling effect causes a local energy transfer from the pole to the equator. Moreover, this local energy transfer introduces the anisotropic distribution of the energy spectrum $e(k, \theta)$ and then the anisotropy of the Reynolds stress tensor. The directional anisotropy directly reflects this anisotropic energy distribution, and then is closely related to the coupling effect.

ACKNOWLEDGMENT

[1] L. Jacquin, O. Leuchter, C. Cambon, and J. Mathieu, "Homogeneous turbulence in the presence of rotation," J. Fluid Mech. **220**, 1 (1990).
[2] N. N. Mansour, C. Cambon, and C. G. Speziale, "Single point modeling of initially isotropic turbulence under uniform rotation," CTR Annual Research Briefs—1991, Stanford University/NASA Ames, 1992, p. 159.
[3] J. Bardina, J. H. Ferziger, and W. C. Reynolds, "Improved turbulence models based on large eddy simulation of homogeneous, incompressible, turbulent flows," Tech. Rep. TF-19, Stanford University, 1983.
[4] A. Salhi and C. Cambon, "An analysis of rotating shear flow using linear theory and DNS and LES results," J. Fluid Mech. **347**, 171 (1997).
[5] J. P. Johnston, R. M. Halleen, and D. K. Lezius, "Effects of spanwise rotation on the structure of two-dimensional fully developed turbulent channel flow," J. Fluid Mech. **56**, 533 (1972).
[6] R. Kristoffersen and H. I. Anderson, "Direct simulations of low-Reynolds number turbulent flow in a rotating channel," J. Fluid Mech. **256**, 163 (1993).
[7] K. Nakabayashi and O. Kitoh, "Low Reynolds number fully developed two-dimensional channel flow with system rotation," J. Fluid Mech. **315**, 1 (1996).
[8] E. J. Hopfinger, *Rotating Fluids in Geophysical and Industrial Applications* (Springer-Verlag, Berlin, 1992), p. 3.
[9] S. Leblanc and C. Cambon, "On the three-dimensional instabilities of plane flows subjected to Coriolis force," Phys. Fluids **9**, 1307 (1997).
[10] C. Cambon, N. N. Mansour, and F. S. Godeferd, "Energy transfer in rotating turbulence," J. Fluid Mech. **337**, 303 (1997).
[11] S. C. Kassinos and W. C. Reynolds, "A structure-based model for the rapid distortion of homogeneous turbulence," Tech. Rep. TF-61, Stanford University, 1994, p. 373.
[12] N. N. Mansour, T. H. Shih, and W. C. Reynolds, "The effect of rotation on initially anisotropic homogeneous flows," Phys. Fluids A **3**, 2421 (1991).
[13] C. Cambon and L. Jacquin, "Spectral approach to non-isotropic turbulence subjected to rotation," J. Fluid Mech. **202**, 295 (1989).
[14] M. Lesieur, *Turbulence in Fluids* (3rd revised and enlarged edition) (Kluwer Academic, Dordrecht, 1997), p. 143.
[15] F. Waleffe, "The nature of triad interactions in homogeneous turbulence," Phys. Fluids A **4**, 350 (1992).
[16] J. R. Herring, "Approach of axisymmetric turbulence to isotropy," Phys. Fluids **17**, 859 (1974).
[17] C. Cambon, D. Jeandel, and J. Mathieu, "Spectral modeling of homogeneous non-isotropic turbulence," J. Fluid Mech. **104**, 247 (1981).
[18] T.-H. Shih, W. C. Reynolds, and N. N. Mansour, "A spectrum model for weakly anisotropic turbulence," Phys. Fluids A **2**, 1500 (1990).
[19] S. A. Orszag and G. S. Patterson, *Numerical Simulations of Turbulence (Statistical Models and Turbulence)*, edited by M. Rosenblatt and C. Van Atta (Springer-Verlag, Berlin, 1972), Vol. 12, p. 127.
[20] W. Polifke and L. Shtilman, "The dynamics of helical decaying turbulence," Phys. Fluids A **1**, 2025 (1989).
[21] Y. Morinishi, K. Nakabayashi, and S. Q. Ren, "Effects of helicity and system rotation on homogeneous decaying turbulence," 3rd International Symposium on Turbulence, Heat and Mass Transfer, Japan, 2000, p. 661.
[22] P. K. Yeung and Y. Zhou, "Numerical study of rotating turbulence with external forcing," Phys. Fluids **10**, 2895 (1998).
[23] L. M. Smith and F. Waleffe, "Transfer of energy to two-dimensional large scales in forced, rotating three-dimensional turbulence," Phys. Fluids **11**, 1608 (1999).
[24] Y. Morinishi, K. Nakabayashi, and S. Q. Ren, "A new DNS algorithm for rotating homogeneous decaying turbulence," Int. J. Heat Fluid Flow **22**, 30 (2001).
[25] K. D. Squires, J. R. Chassonov, N. N. Mansor, and C. Cambon, "Investigation of the asymptotic state of rotating turbulence using large-eddy simulation," CRT Annual Research Briefs—1993, Stanford University/NASA Ames, 1994, p. 157.
[26] Y. Murakami, L. Shtilman, and E. Levich, "Reducing turbulence by phase juggling," Phys. Fluids A **4**, 1776 (1992).
[27] F. Waleffe, "Inertial transfers in helical decomposition," Phys. Fluids A **5**, 677 (1993).